wind

MDPI

Article

Wind Effects of Surrounding Structures in an Urban Area on a High-Rise Building by Computational Fluid Dynamics

Citlali Villalobos-García, Luis Francisco Pérez-Moreno, Iván Fermín Arjona-Catzim and Enrique Rico-García *

Facultad de ingeniería, Universidad Autónoma de Querétaro, Querétaro 76000, Mexico; cvillalobos09@alumnos.uaq.mx (C.V.-G.); lf.perezm@uaq.mx (L.F.P.-M.); ivan.arjona@uaq.mx (I.F.A.-C.)
* Correspondence: ricog@uaq.mx

Abstract

Wind design aims to ensure the stability, safety, and durability of a structure exposed to wind forces. This comparative study using Computational Fluid Dynamics (CFD) was conducted to evaluate the effects of surrounding structures in wind building design. Two scenarios were analyzed: the first, in which the building was exposed to an open field, and the second, in which the building was surrounded by other buildings of equal or lower height. A CFD model, previously calibrated with experimental data, was used to simulate wind behavior. The results obtained showed significant differences between the two scenarios, confirming that nearby structures have a considerable impact on the distribution of wind pressures on the building. Therefore, the importance of considering surrounding buildings is highlighted. CFD could be a useful complementary tool for obtaining pressure coefficients and for detailed analyses of wind behavior, which could improve the design and safety of buildings under wind loads.

Keywords: CFD; pressure coefficients; turbulence; velocity profile; wind effects; surrounding buildings

1. Introduction

In structural engineering, one of the principal objectives is to produce a design that guarantees the security, resilience, and durability of the structure. All loads that can influence the structure must be considered [1], such as dead loads, live loads, and accidental loads. Accidental loads are those that can emerge suddenly and act during a short period of time, but their presence can harm the stability of the structure, such as the effects of earthquakes, snow loads, and wind [2]. Countries such as Germany, France, the United Kingdom, and Mexico are severely exposed to wind action, and there has been damage to buildings as a result [3].

Wind is a fluid that can damage structures when they are exposed to high wind speeds, causing economic losses [4]. Wind effects are very difficult to replicate perfectly due to vorticity effects and turbulence flows. The pressure coefficients and pressures that impact a structure must also be obtained [5]. Analyzing wind effects requires experimental studies such as those using wind tunnels and full-scale measurements; in both cases, expensive tools are required in addition to careful calibration. In wind tunnels, scaled models with real fluids are studied [6].

To determine wind effects on a structure, standards such as those from the Eurocode (NE-EN 1991-1-4) [7], Normas Técnicas Complemetarias para Diseño por Viento (NTC-2023) [8], and American Society of Civil Engineers (ASCE 7) [9] are used. In general, these

Check for updates

Academic Editors: Mihail Iancovici and Firoz Alam

Received: 14 January 2026
Revised: 13 March 2026
Accepted: 19 March 2026
Published: 2 April 2026

Copyright: © 2026 by the authors. Licensee MDPI, Basel, Switzerland. This article is an open access article distributed under the terms and conditions of the Creative Commons Attribution (CC BY) license.

codes present a methodology to estimate pressure coefficients over the surface of a structure; however, these values are constant even in the presence of surrounding structures [10].

In wind design, it is necessary to know the characteristics of the zone, such as the rugosity of the land. Studies have demonstrated that in urban areas, the presence of other structures has a strong influence on wind effects, while increased rugosity reduces the wind velocity but generates other effects such as turbulence and vorticity [11,12]. Analyzing an urban area is very complicated due to the effects that are generated and the instability of flow. It is important to take into account parameters such as the burst factor, which relates the maximum velocity of the wind in the area and medium flow, allowing extreme conditions to be evaluated [13].

Wind tunnel tests have been conducted to evaluate wind behavior in dense urban environments. These studies consider a building with a regular geometry surrounded by square buildings aligned in rows with small gaps. The findings indicate that pressure coefficients, forces, and moments change significantly depending on the height, shape, and distance between nearby buildings [14–16].

Urban areas are increasingly large, and with that, the number of high-rise buildings is growing. Through structural engineering, these buildings are designed to resist high loads from winds [17]. Therefore, it is important to study wind effects on urban areas. Currently, with advances in technology, various strategies have been employed for this type of study with the implementation of software and mathematical models.

CFD (Computational Fluid Dynamics) is a branch of fluid mechanics that analyzes highly complex fluid problems using mathematical models and computers, based on the laws of conservation [18–20]. This is used to analyze fluids such as wind, for which studies have demonstrated that the good performance of CFD in predicting wind effects relies on the geometry, type of mesh, orthogonal quality, turbulence model, and solution method [21]. In [22], a series of processes based on parameters were obtained from the state of the art and from the general configuration of CFD, that is, pre-processing; setting the geometry, meshing, and initial and boundary conditions; choosing the solver; setting the models and precision of the analysis; and, finally, obtaining results.

Studies have shown that the presence of surrounding structures influences the precision of the wind path prediction, not only through the distribution of pressure coefficient patterns but also through the magnitude of the forces. In addition, some standards overestimate or underestimate pressure changes when the zone is dense [23,24]. Table 1 presents a compilation of studies in which CFD has been used and criteria have been found to evaluate its veracity.

Table 1. A collection of studies illustrating the state of the art.

Title	Comment	Ref
Evaluating the wind loads on high-rise buildings of various plan dimensions through numerical simulations.	Checked the functionality of CFD for capturing pressure coefficients for high-rise buildings via WMLES simulations, which are more precise than RANS models.	[25]
Experimentally estimating wind load coefficients for tornadoes—An alternative perspective.	Explained the importance of turbulence and its relationship with applied loads on a surface or structure.	[26]

Table 1. *Cont.*

Title	Comment	Ref
A technical review of computational fluid dynamics (CFD) applications on wind design of tall buildings and structures: Past, present and future	Parameters such as the velocity profile, mean pressure turbulence intensity profile, turbulence model, and solution method influence the pressure for obtaining pressure coefficients on a surface. The LES model is more accurate than RANS but has higher computational costs.	[27]
CFD simulation advances in urban aerodynamics: Accuracy, validation, and high-rise building applications	Turbulence models such as k-ε-RNG and SST-ω-Standard were compared, including parameters like kinetic energy and the dissipation rate. To validate this research, wind tunnel studies were used. The result was that both models are reliable, but the k-ε model has a lower computational cost.	[28]

CFD, in wind engineering, is used to conduct studies that analyze the effects of wind at the pedestrian level to evaluate pedestrian comfort and to avoid possible economic losses due to gusts [29]. Besides this, some studies have focused on the effects of wind on high-rise buildings, while others have analyzed wind behavior in the presence of vegetation and the associated air quality.

The objective of this study was to evaluate, using CFD, the influence of surrounding structures on the pressure coefficients of a tall building in an urban environment, reproducing the real conditions of the site and comparing the results with wind tunnel tests.

2. Materials and Methods

For this study, two scenarios were developed: the first was CFD model calibration with experimental data, such as that from wind tunnel tests and full-scale samples, where the building is surrounded by buildings of equal or lesser height in an urban area; the second, based on the considerations of the first, examined only a completely isolated building exposed in an open field. The ANSYS Fluent R1 2023 software was used for this study.

The reference experimental data were taken from the work of Kikuchi et al. [30]. This study employed an atmospheric boundary layer (ABL) wind tunnel measuring 2 m wide by 16 m long. To simulate urban environment conditions, 1/500 scale models were used, covering a 500 m radius around the center of the building under analysis, maintaining a blocking rate of less than 5%. The terrain was classified as Category III (suburban wooded with few tall trees).

2.1. Scenario 1

For this case, a tall, regular building in a dense urban area surrounded by structures of equal or lesser height was examined; therefore, the structures closest to the study building were considered. The methodology is described below for the three phases of the CFD model used for this first scenario.

2.1.1. Pre-Processing, Scenario 1

The object of study in this research is a regular-shaped high-rise building with a floor plan measuring 59.4 × 59.4 m and a height of 155 m (Figure 1), located in the city of Yokohama, Japan. The building is surrounded by 12 structures of equal or lesser height. Data was obtained regarding its geometry, and experimental results, such as those from wind tunnel tests and full-scale measurements, were obtained from a study conducted by Kikuchi et al. [30]. The dimensions and coordinates of the surrounding buildings are described in Appendix A.1.

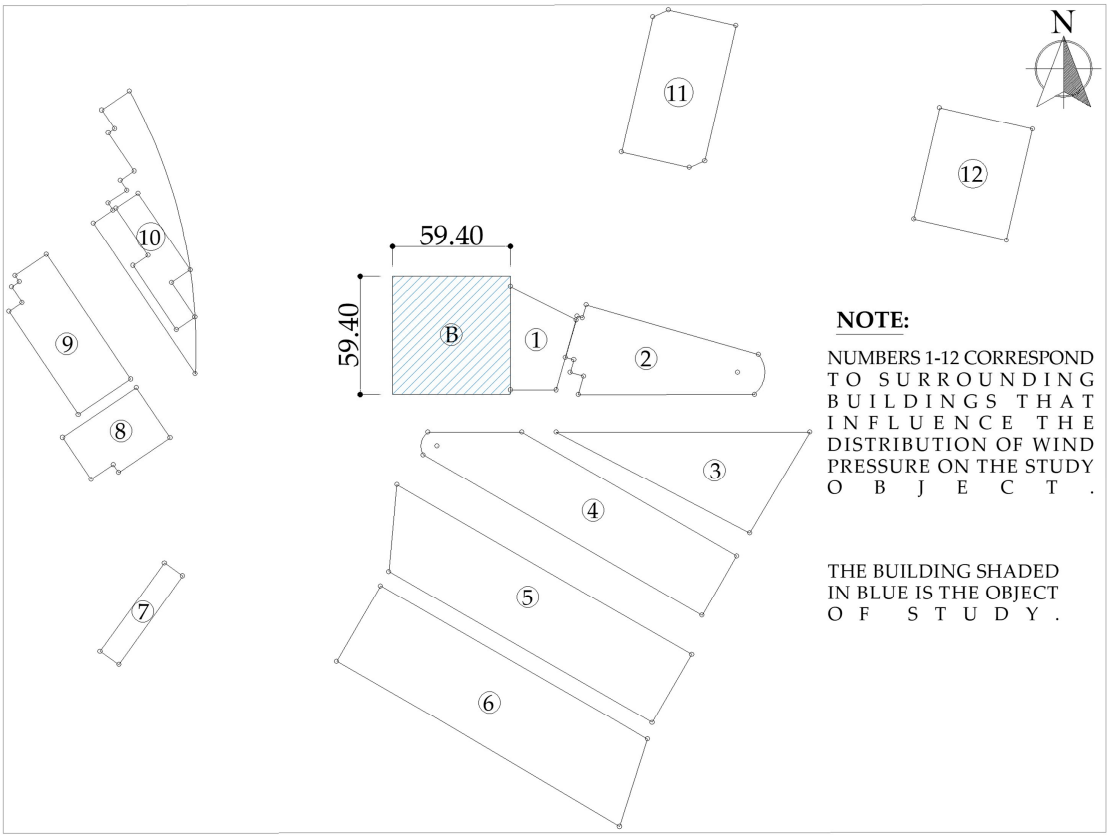


Figure 1. The dimensions of the considered buildings. The heights of the buildings are as follows: B, 155 m; 1, 23 m; 2, 100 m; 3, 65 m; 4, 65 m; 5, 65 m; 6, 65 m; 7, 60 m; 8, 100 m; 9, 110 m; building 10 consists of two different sections, but the total height of the building is 100 m; 11, 150 m; 12, 140 m.

For the scenario in which the building under study is surrounded by other buildings, approximate measurements were used to develop the geometry of the surrounding buildings. The floor plan measurements are shown in Figure 1.

In developing the domain, the dimensions were taken in relation to the size of the building (object of study), where its height was defined as H and the sides of the building, being symmetrical, were defined as having length L. The dimensions of the domain were established as shown in Figure 2a, with measurements taken from the limits of the surrounding buildings.

For scenario 1, the flow inlet was in the front zone of the domain at 6L from the limits of the surrounding structures. For the side edges and the top edge, a symmetry condition was applied, indicating that the flow was continuous over those limits, as shown in Figure 3.

The meshing techniques applied for this study were validated against the results of experimental studies, where model calibration was performed by evaluating two turbulence models (k-ε and k-ω-SST) with two different types of meshes (polyhedra and polyhexacore) and two solution methods (simple and coupled). The result of this process was that the most accurate simulation with respect to experimental results was the configuration of a k-ω-SST turbulence model with the simple solution method and a polyhexacore mesh, because it adapted better to irregular surfaces and its hexacore elements reduced the computational cost by coupling optimally to the rest of the domain [31]. The configurations used for the two types of meshes evaluated here are described below.

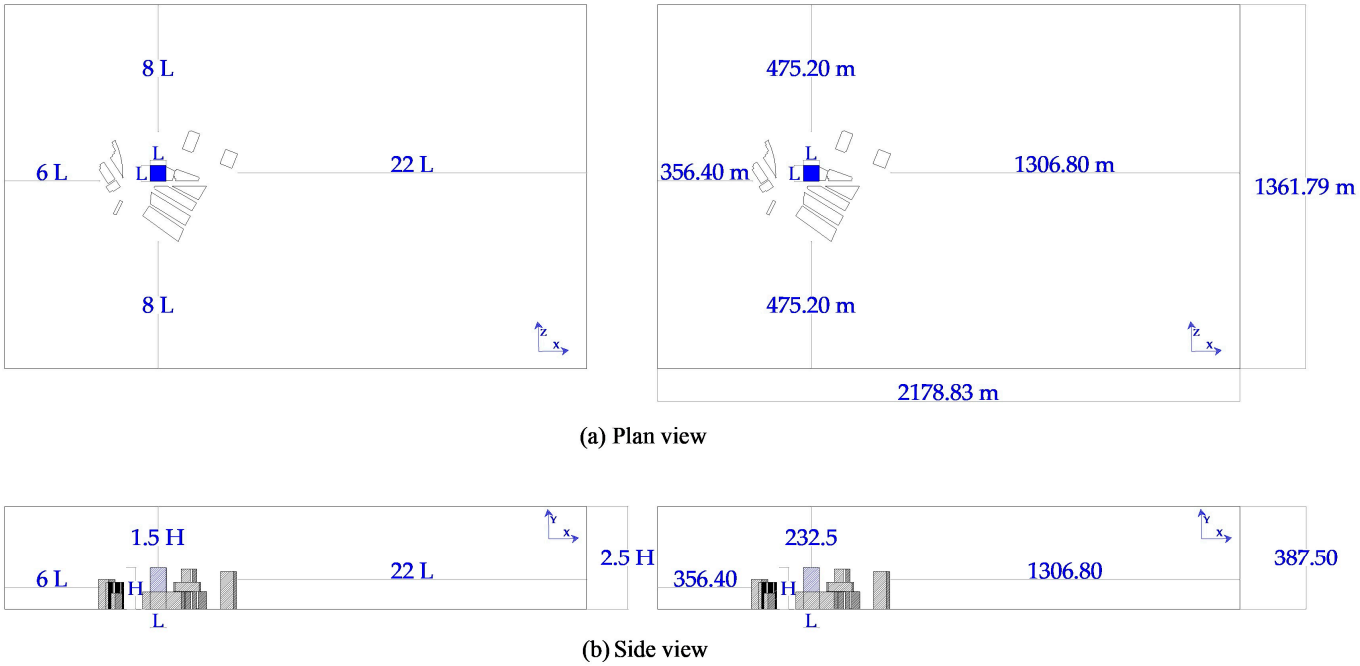


Figure 2. The domain dimensions of scenario 1, a building with surrounding structures: H: 155 m (building height), L:54.9 m (building sections).

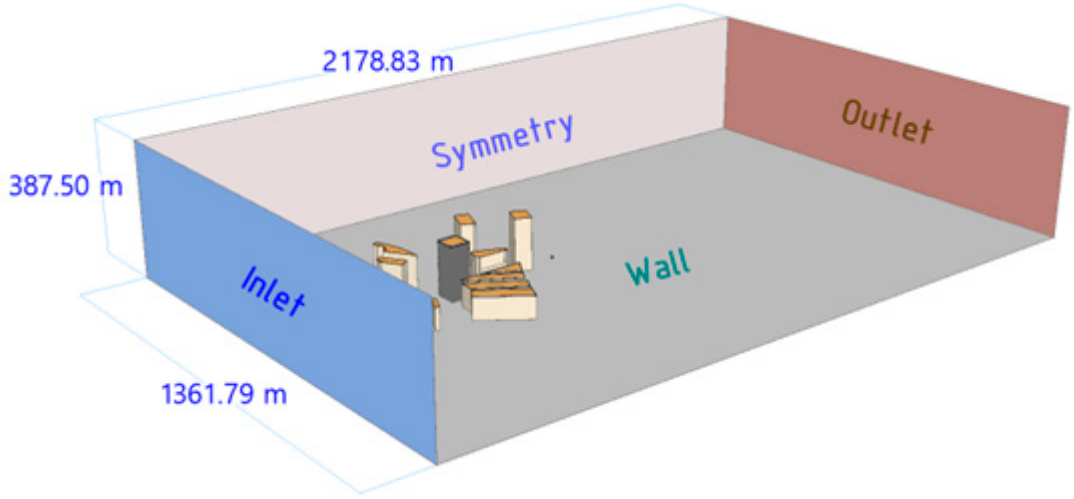


Figure 3. Boundary conditions and domain dimensions of scenario 1.

Polyhedra: The mesh size of the building was first obtained as 1% of the building's height, that is, 1% of 155 m, resulting in a total of 1.5 m. This simplified the model and reduced the number of elements, thereby lowering the computational cost. Furthermore, it facilitated detailed coverage of the area of interest, as the mesh size was relatively small compared with the domain size [32].

A local face size was applied with respect to the building of interest, unifying the building's mesh size with a local size of 1.5 m. Additionally, local region refinement was applied to achieve greater accuracy in data acquisition by refining the mesh around the walls of the building of interest. The final mesh size was defined as 7.75 m, over five times the mesh size of the building of interest. For the overall mesh size, a size of 15 m was defined with a growth rate of 1.1, to avoid abrupt changes in the mesh size.

For these analyses, boundary layers must be added; these layers generate a roughness effect on the fluid when it impacts a solid surface. The number of layers used for a study depends on whether the flow being analyzed is turbulent according to the Reynolds number,

as shown in Equation (1). If the flow is not turbulent, the boundary layer requires a greater number of layers than if it is turbulent [19]. The Reynolds number in this case was greater than 4000, indicating turbulent flow. Therefore, a thin boundary layer was required. The flow was confirmed to be turbulent, and thus, 10 layers were assigned with a growth rate of 1.1, which corresponds to a discrete increment factor.

$$\mathrm{Re} = \frac{\mathrm{V.L}}{\mathrm{v}} \quad (1)$$

Here,

V: reference velocity (m/s);
L: impact length (m);
ν: fluid viscosity (m^2/s).

The overall mesh volume was generated with a growth rate parameter of 1.1 to avoid abrupt size transitions, and an overall size of 12.2 m was assigned because the 15 m size resulted in poor mesh quality with an orthogonal quality of 0.01. Ultimately, with the modifications made, a mesh with an orthogonal quality of 0.45 was obtained, which corresponds to acceptable mesh quality [33].

Polyhexacore: Local sizing was applied to the building of interest, unifying the building's mesh size with a local size of 1.1 m. Subsequently, local refinement regions were added. The mesh size was defined as 3 m, over three times the building's mesh size.

For the overall mesh size, a size of 10 m was defined with a growth rate of 1.2 to avoid abrupt changes in mesh size.

The Reynolds number was checked, resulting in a value greater than 4000, indicating turbulent flow. Therefore, 10 boundary layers were assigned with a growth rate of 1.1, corresponding to a discrete increment factor, thus avoiding abrupt changes.

A total mesh size of 10 m was established with a growth rate of 1.1 because a mesh size of 15 m resulted in a poor mesh quality of 0.01. Finally, by applying an Improve Volume Mesh, a mesh with an orthogonal quality of 0.46 was obtained.

An exponential wind velocity profile was used due to its simplicity of expression (Equation (2)) since this contributes to the precision of the simulation [34].

$$V_z = V_{ref}\left(\frac{Z}{Z_{ref}}\right)^{\alpha} \quad (2)$$

Here,

V_z: wind velocity to be estimated at height Z above ground level (m);
V_{ref}: reference velocity (m/s);
Z: height variation;
Z_{ref}: height related to the reference speed (m);
α: roughness exponent (Table 2).

Table 2. Roughness exponent values [35].

Parameter	Value
Water	0.13
Grass	0.14–0.16
Crops and shrubs	0.20
Forests	0.25
Urban area	0.40

Note: For this study, the value of α is 0.40 because the building is in an urban area with many buildings of equal or lesser height.

Due to this study's sensitivity, input parameters such as kinetic energy k (3) and the specific dissipation rate ω (5), which relate to the atmospheric boundary layer (ABL) of wind profiles, were considered to include more realistic parameters [23].

$$k = \frac{{u^*_{ABL}}^2}{\sqrt{C\mu}} \tag{3}$$

Here,

u^*_{ABL} : friction velocity;
$C\mu$: empirical coefficient, equal to 0.09.

Likewise, equations were added to complement the analysis in this study, such as those for the turbulent energy dissipation rate ϵ (4) and friction velocity u^*_{ABL} (6). These parameters are described later in this paper with respect to the conditions of the area in which the building is located.

ϵ is the turbulent energy dissipation rate [m^2/s^3] [36],

$$\epsilon = \frac{{u^*_{ABL}}^3}{\kappa(z + z_0)} \tag{4}$$

where

u^*_{ABL} : friction velocity;
κ: Von Karman constant, equal to 0.4;
z: height variable [m];
z_0: terrain roughness height, equal to 1 m.

ω is the specific dissipation frequency [1/s] [37],

$$\omega = \frac{\epsilon}{kC\mu} \tag{5}$$

where

ϵ: turbulent energy dissipation rate [m^2/s^3];
$C\mu$: empirical coefficient, equal to 0.09;
k : kinetic energy.

u^*_{ABL}, the friction velocity [m/s], represents the velocity profile affected by roughness:

$$u^*_{ABL} = 0.4\frac{V_{ref}}{\ln\left(\frac{z_0 + z_{ref}}{z_0}\right)} \tag{6}$$

where

u^*_{ABL} : friction velocity;
V_{ref}: reference wind velocity [m];
z_{ref}: reference height [m];
z_0: terrain roughness height, equal to 1 m.

2.1.2. Solution, Scenario 1

The solution model was a k-ω-SST model, as its calibration provided a better fit for capturing fluid effects on the surface. This was in reference to CFD tests performed to evaluate and calibrate the model, the results of which have not yet been published. The solution method was simple, solving the Navier–Stokes equations by coupling the fluid pressure and velocity; 1000 iterations were used because within that range of iterations, the flow behavior becomes constant with respect to the residual graph.

2.2. Scenario 2

2.2.1. Pre-Processing, Scenario 2

In the second scenario, the dimensions were established with respect to the dimensions of the building (Figure 4); in addition, the building was considered completely exposed to the effects of the wind, without any disturbances that could influence the distribution of the pressure coefficients.

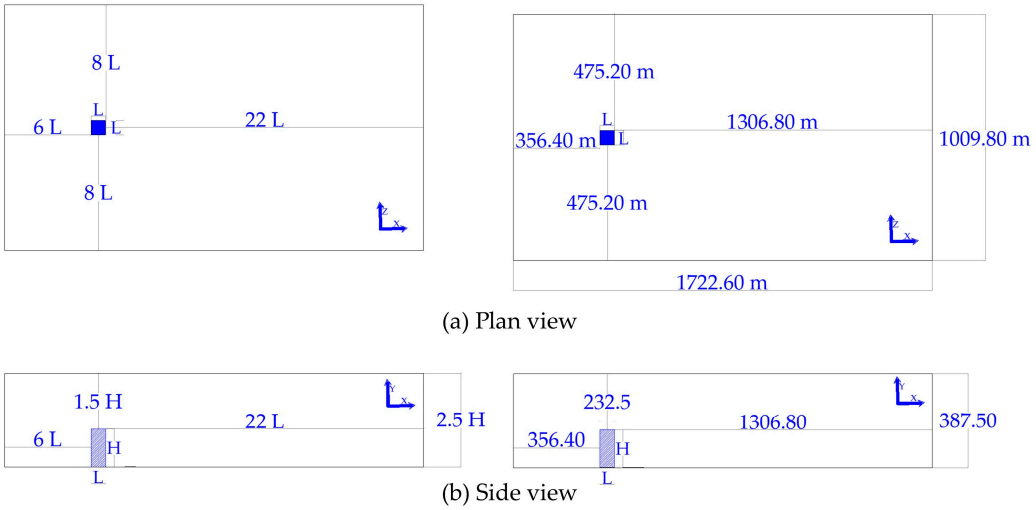


Figure 4. The domain dimensions of scenario 2, a building in an open field: H: 155 m (building height), L: 54.9 m (building sections).

To define the boundary conditions, the entrance to the front zone of the domain was set at 6L with respect to the limits of the building. The sides and the top of the domain were considered with a condition of symmetry, considering that the fluid was still continuous on those edges. The bottom of the domain was established as a wall (Figure 5).

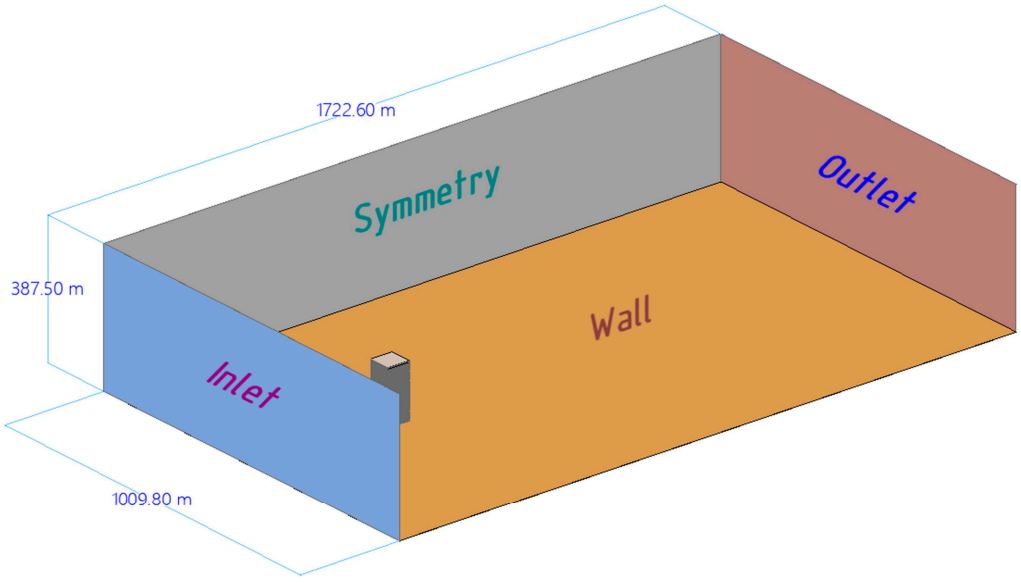


Figure 5. Boundary conditions: scenario 2, a building exposed to open countryside.

For Scenario 2, the results obtained through calibration were considered, and a poly-hexacore mesh type was generated. The meshing technique that was applied was in relation to the height of the building. To obtain the mesh size on the walls of the building, the criterion was set to 1% of the height of the building, corresponding to 1.5 m. However, to

avoid deformations on the elements, it was taken as a value at 0 decimal places, and thus, the final mesh size on the edge of the building was 1 m.

Local sizing was applied to the building of interest, unifying the building's mesh size with a local size of 1 m. Additionally, local region refinement was implemented to improve the data acquisition accuracy by refining the mesh relative to the building's walls. The mesh size was defined as 10 m, 10 times the size of the building's mesh, to reduce computational costs.

For this scenario, the reference wind velocity value with respect to the height of the building corresponds to 1.51 m/s; the viscosity of the flow corresponds to that of air, with a value of 1.5×10^{-5} m^2/s; and by solving the equation, it was verified that such flow is completely turbulent. Therefore, only 5 layers were used on the wall conditions, with a growth rate of 1.2 to avoid sudden changes in each of the levels of the layer. The height of the first boundary layer was 0.272 m, and at the end of the process, an orthogonal quality of 0.5 was obtained.

2.2.2. Solution, Scenario 2

Steady state solutions and a k-ω-SST turbulence model, with a simple solution method, were used, with 1500 iterations performed. Variables established in Table 3 were introduced.

Table 3. Input conditions and variables.

Parameter	Value
Inlet velocity	1.51 m/s
Outlet pressure	0 Pa
Wall	No-slip
Air density	1.255 kg/m^3
Air viscosity	1.5×10^{-5} m^2/s
Wind velocity	V_z (Equation (2))
Kinetic energy	k (Equation (3))
Turbulent energy dissipation rate	ϵ (Equation (4))
Specific dissipation frequency	ω (Equation (5))
Friction velocity	u^*_{ABL} (Equation (6))

Note: The parameters used for CFD simulations with a k-ω-SST turbulence model.

3. Results

The characteristics of six polyhexacore mesh types are presented, as the mesh type analysis and solution model evaluation indicated that this mesh was ideal for this study, as shown in Table 4. Associated graphs can be viewed in Appendix A.2. The first three meshes correspond to scenario 2, where the building is exposed to open fields, and meshes 4, 5, and 6 correspond to scenario 1 The evaluation condition to determine if a mesh is good indicates that the orthogonal quality must be greater than 0.4 and it is considered an acceptable mesh [33].

Table 4. Mesh characteristics.

Mesh	Total Number of Cells	Minimum Orthogonal Quality	Maximum Aspect Ratio	Maximum Skewness
1	2,191,351	0.50	49.38	0.21
2	2,264,594	0.50	18.21	0.45
3	2,627,127	0.50	19.21	0.44
4	3,254,540	0.45	34.20	0.92
5	2,560,055	0.48	40.90	0.85
6	2,560,362	0.42	23.39	0.63

Note: Polyhexacore meshes were evaluated for scenarios 1 (meshes 4, 5, and 6) and 2 (meshes 1, 2, and 3).

The graph in Figure 6 presents an evaluation of the simultaneity of pressure coefficients for both scenarios; it can be observed that the mesh density no longer influenced abrupt changes in the obtained pressure coefficients.

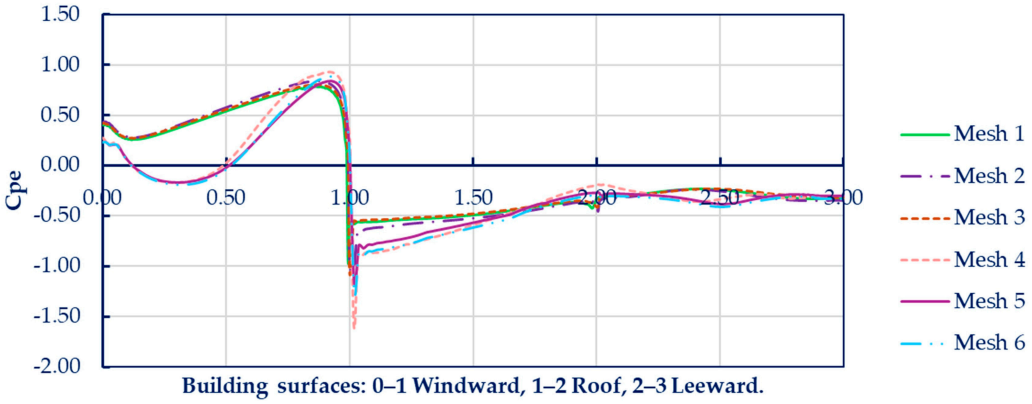


Figure 6. Mesh independence. It is observed that the mesh size density does not significantly affect the obtaining of pressure coefficients.

Figure 7 shows representations of the profiles used for the CFD model solution: (a) the wind speed profile, obtained from Equation (2); (b) the dissipation frequency profile (Equation (5)); and (c) the turbulent dissipation rate profile (Equation (4)).

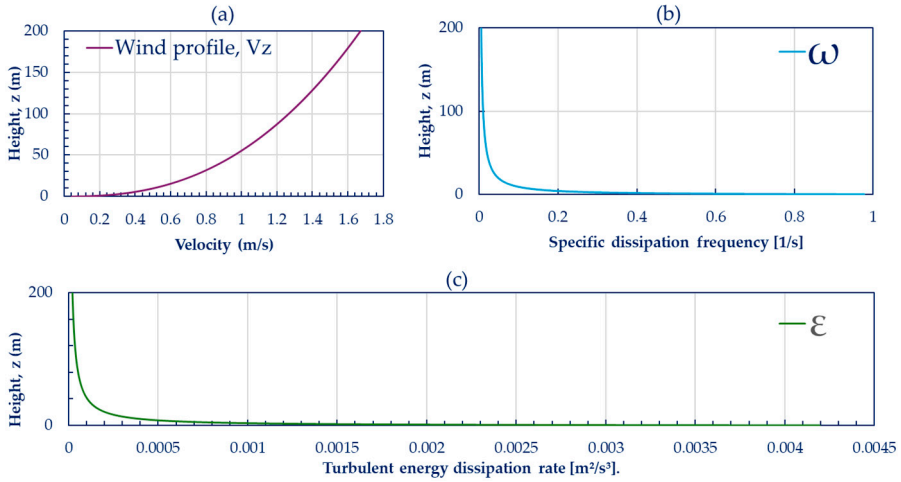


Figure 7. Profiles used for CFD model solution: (**a**) wind speed; (**b**) dissipation frequency; and (**c**) turbulent energy dissipation rate.

3.1. Results, Scenario 1

The CFD model of scenario 1, where the building is surrounded by structures that alter the wind's trajectory and cause it to directly impact the leeward side, yielded results like those obtained through experimental studies using wind tunnels and full-scale samples. Figure 8 shows a comparison between scenario 1 and experimental results, focusing on the windward side. The percentage of similarity in this comparison was greater than 80%.

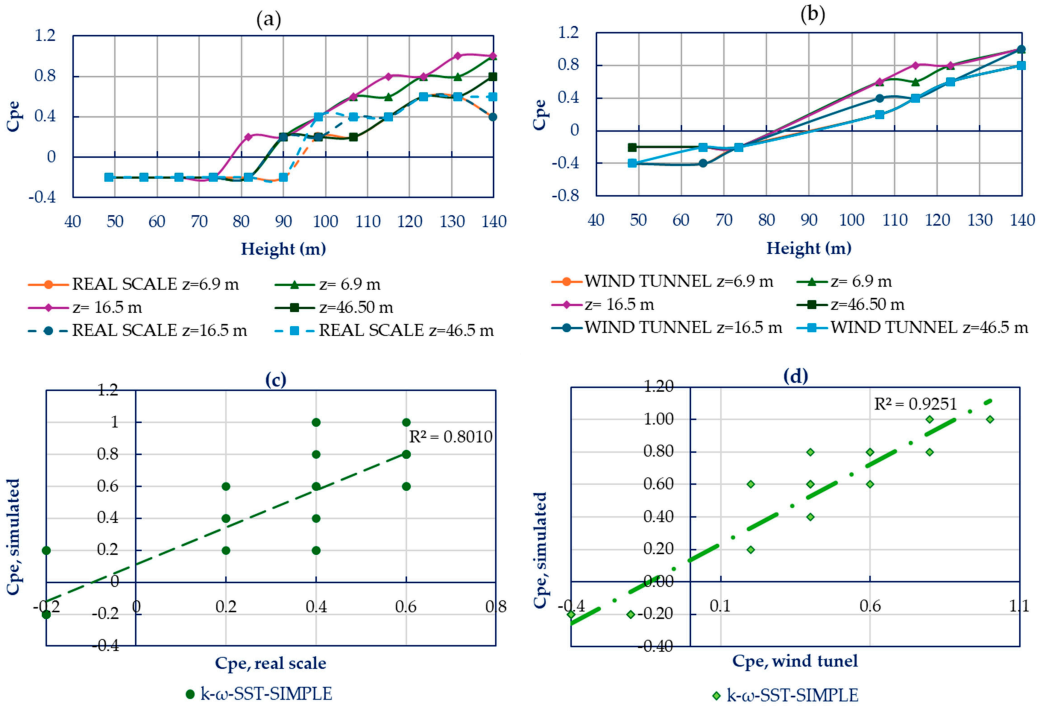


Figure 8. Comparisons of pressure coefficients obtained from scenario 1 on the windward side: (**a**) simulated Cpe vs. actual scale, (**b**) simulated Cpe vs. wind tunnel, (**c**) a linear model to determine the percentage of similarity between CFD and actual scale results, and (**d**) a linear model to determine the percentage of similarity between CFD and wind tunnel results.

3.2. Results, Scenario 2

For scenario 2, where the building is considered without the presence of surrounding structures that could influence the distribution of pressure coefficients on the building faces, as in current wind design regulations, the results show variability with respect to the pressure coefficients obtained in experimental studies.

Figure 9a shows that when the results obtained using the CFD model are compared with those obtained in experiments carried out on a real scale, the difference in the distribution of pressure coefficients is variable; this is also the case in Figure 9b, where the results are compared with pressure coefficients (Cpe) obtained in a wind tunnel experiment. This highlights the importance of considering the surrounding structures.

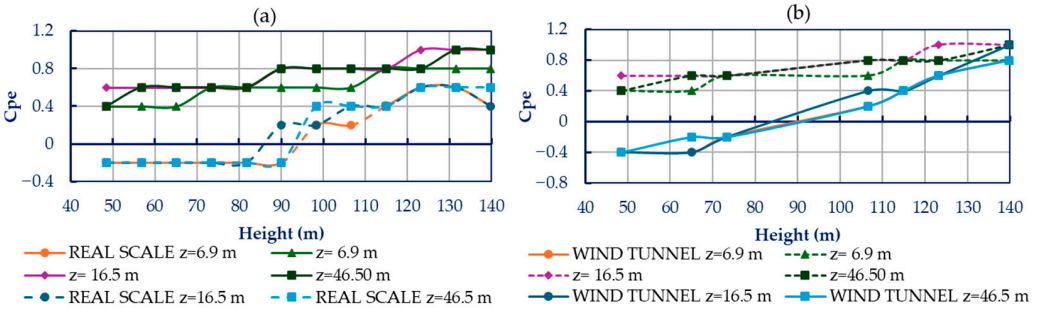


Figure 9. Comparisons of pressure coefficients obtained from scenario 2 on the windward side: (**a**) simulated Cpe vs. actual scale; (**b**) simulated Cpe vs. wind tunnel.

4. Discussion

This study illustrates the difference in the pressure coefficient distributions obtained when surrounding structures are present and when they are absent. In a building in an open field, on the windward side, the pressure coefficient increases with the height of the structure, and the values are positive, indicating direct pressure on the building. In

contrast, for a building surrounded by structures, the distribution changes with respect to the height of the surrounding structures and that of the building itself, with the coefficients varying in value from negative values, representing suction, to positive values, indicating direct pressure.

Figure 10 shows the variation in the pressure coefficients with respect to the height of the building (H) at distance z above the face of the building.

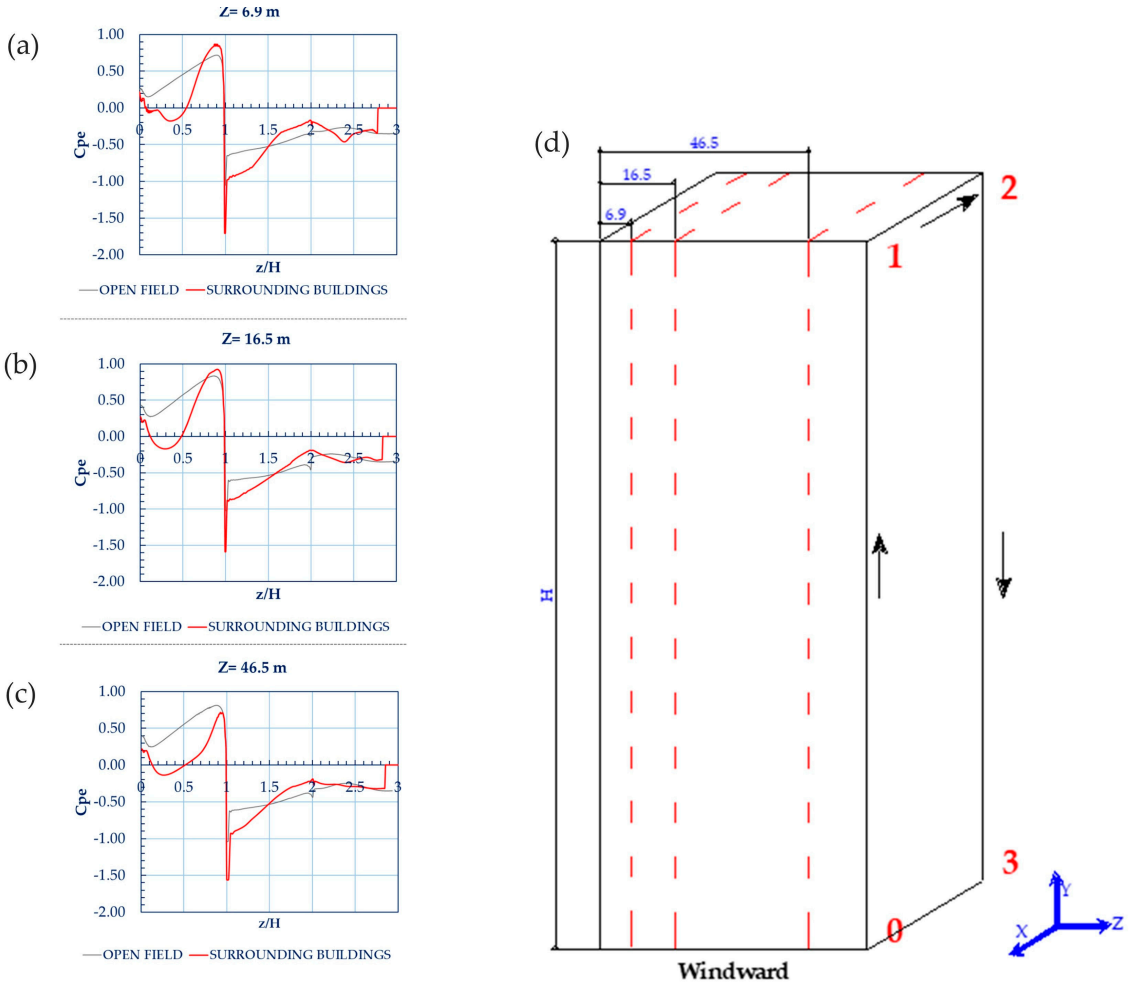


Figure 10. Distributions of pressure coefficients (Cpe) with respect to height. (**a**) Vertical profile at Z = 6.9 m. (**b**) Vertical profile at Z = 16.5 m. (**c**) Vertical profile at Z = 46.5 m. (**d**) Schematic representation of the building indicating the positions of the three vertical profiles (dotted red lines) on the windward (0−1), roof (1−2) and leeward (2−3) faces. Arrows indicate the analysis sequence.

The distribution of pressure coefficient values varies not only with respect to the height of the structure but also with respect to the length of the building face (Figure 11). Furthermore, the presence of surrounding buildings influences not only the windward face but all four faces of the building.

In Figure 11a, it can be observed that when wind directly impacts the structure, the coefficient values increase with the height of the building and in places approaching the edges of the building face. In the case where surrounding structures prevent the direct impact of wind, suction effects are generated, resulting in pressure coefficient values that vary from −0.10 in the windward case to 0.9, with a non-constant distribution depending entirely on the particular obstructions.

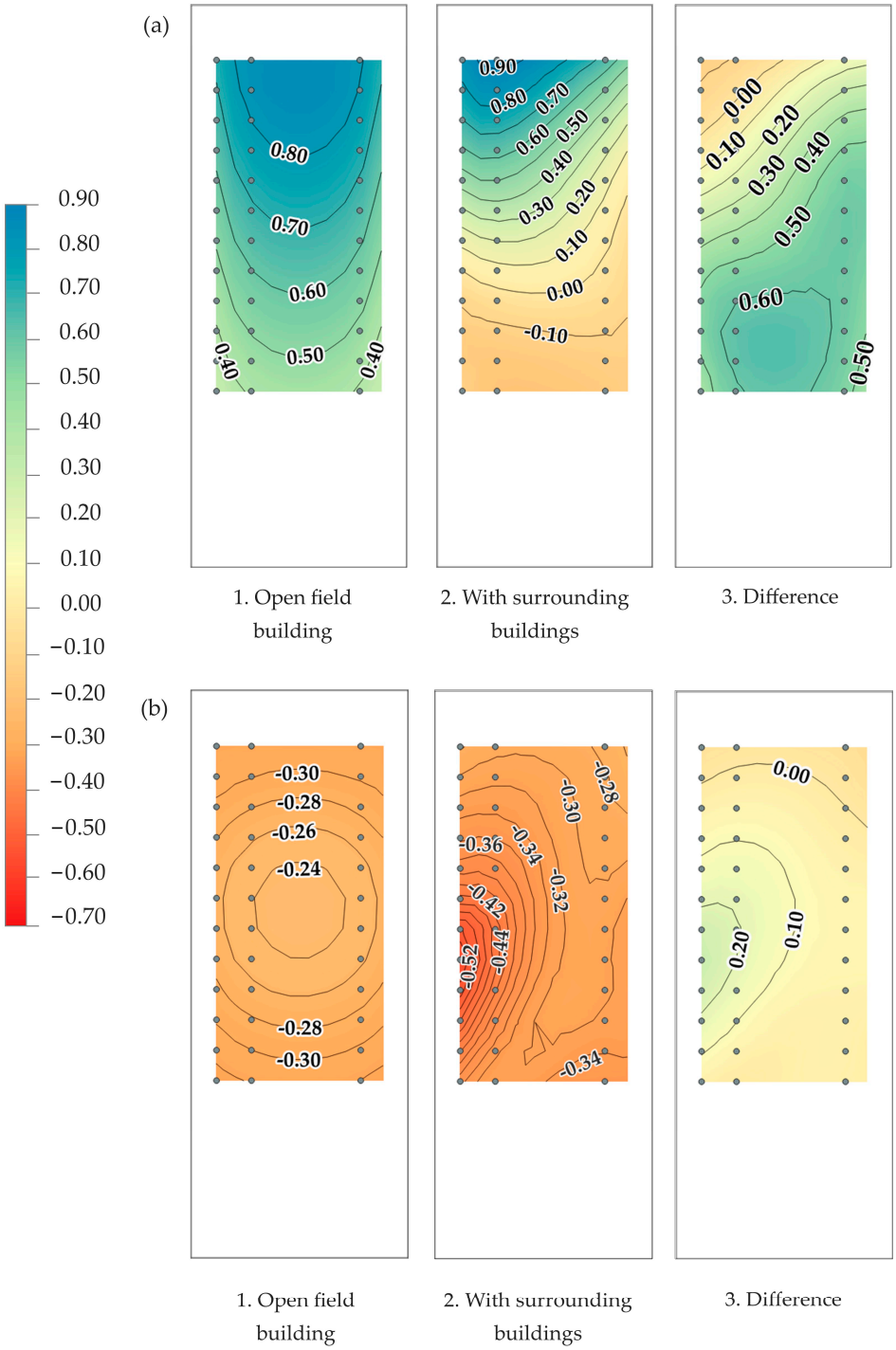


Figure 11. Pressure coefficient distributions for when the building is located in an open field and when it is surrounded by structures of equal or lesser height: (**a**) windward side; (**b**) leeward side.

In Figure 12a,b, the pressure coefficient distributions on both side faces are similar when it comes to scenario 2. However, when there are obstructions that disturb the path of the wind, generating vortices and suction, the distribution is variable with respect to the quantity and size of the surrounding structures. The behavior in both cases is different with respect to the distributions, though not so much with respect to the values.

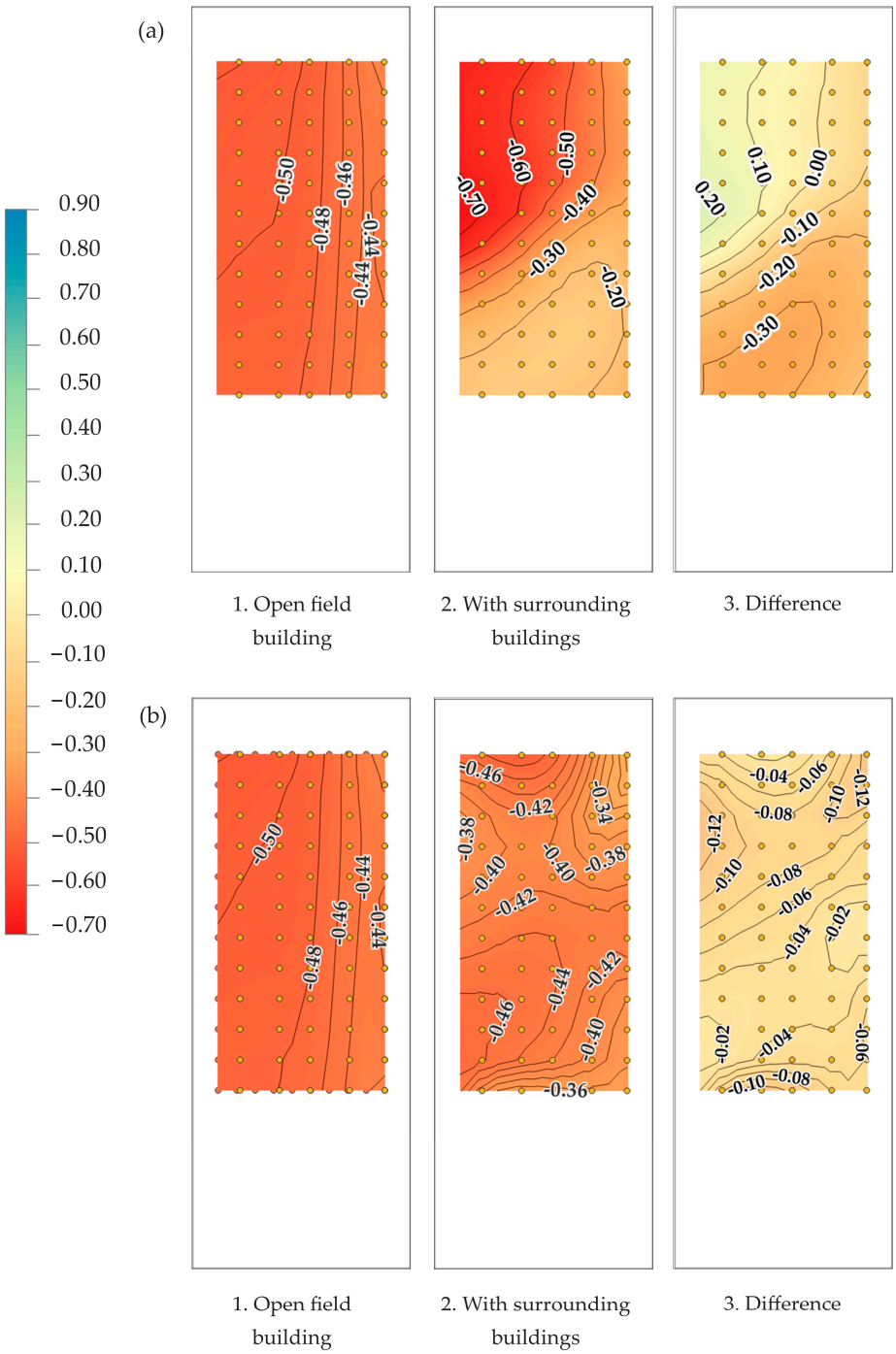


Figure 12. Pressure coefficient distributions on the lateral faces when the building is located in an open field and when it is surrounded by structures of equal or lesser height: (**a**) lateral 1, north-facing; (**b**) lateral 2, south-facing.

In this case, although these are not the faces receiving the greatest impact from the wind, the impacts are significant due to suction effects. However, it was also observed that although there should be greater impacts on the four faces of the building in an open field, the presence of the surrounding buildings influences not only the distribution but also the obtained values of the pressure coefficients on the structure.

In Figure 13a, the similarity between the two models ranges from 19% to 4%, with values being more similar when obstructions do not directly affect the structure. In the case of (b), for the leeward side, the similarity between the pressure coefficient distri-

butions differs considerably, ranging from 96% to 47%, highlighting the importance of surrounding structures.

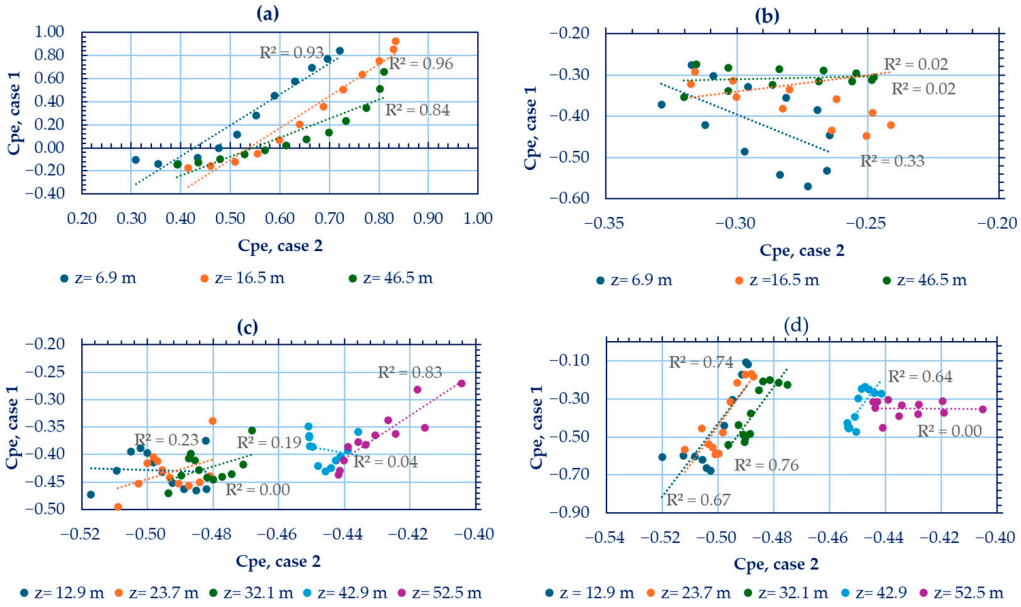


Figure 13. Linear models to obtain the percentages of simultaneity between the cases by means of the coefficient of determination (R^2) for the 4 sides of the building: (**a**) windward, (**b**) leeward, (**c**) Side 1, and (**d**) Side 2.

The same applies to the laterals, where the coefficient of determination shows variability when both cases are compared. The cases show a difference of 100% to 17% for the laterals, where at a distance of 52.5 m from the x-axis, the pressure coefficient distributions do not coincide due to the influence of the surrounding structures.

Although the most damaging scenario for a structure affected by wind is that in which it is exposed in an open field, through this study, it was observed that the values were significantly different. In addition, some regulations for the static effects of wind on a structure consider constant pressure coefficients on each of the faces, which generalizes the methodology but also neglects the presence of other structures. Thus, it would also be important to carry out a study through CFD as a complementary tool for wind design in structures, although it is necessary to have adequate equipment to improve the computational cost of the simulations. Real or scale measurements of the study area should also be considered to produce better results.

Furthermore, although some regulations do not validate the use of CFD for this type of study, Eurocode suggests CFD as a usable tool under certain conditions [7].

5. Conclusions

The results obtained using CFD as an analysis tool show that for this and some other cases, it is important to consider the presence of surrounding structures when analyzing wind effects. Surrounding structures can modify the distribution of pressure coefficients on building faces, resulting in an average overall reduction of 27% in this study. Although the most unfavorable scenario is considered to be when a building is exposed to open terrain, this study revealed that ignoring the presence of surrounding structures would be a mistake. In open terrain, the windward side receives only positive pressure or thrust. However, the presence of surrounding structures can lead to both thrust and suction generated on the windward side due to wind interference effects.

For future research, it is recommended to evaluate the effect of the wind's angle of incidence by varying the flow direction, and to analyze the influence of the location, height, and shape of surrounding buildings.

These aspects are essential since in the present study, the height, geometry, and position of the target building remained constant; even so, the distribution of the pressure coefficients changed substantially due to the presence of upstream structures obstructing and redirecting the incident flow.

Author Contributions: Conceptualization, C.V.-G. and E.R.-G.; methodology, C.V.-G. and E.R.-G.; validation, C.V.-G. and E.R.-G.; formal analysis, C.V.-G. and E.R.-G.; investigation, C.V.-G.; resources, C.V.-G.; data curation, C.V.-G. and E.R.-G.; writing—original draft preparation, C.V.-G.; writing—review and editing, E.R.-G.; writing—review and editing, I.F.A.-C. and L.F.P.-M. All authors have read and agreed to the published version of the manuscript.

Funding: This research did not receive external funding.

Institutional Review Board Statement: Not applicable.

Informed Consent Statement: Not applicable.

Data Availability Statement: The original contributions of the paper are contained in the manuscript, and other queries can be forwarded to the corresponding author.

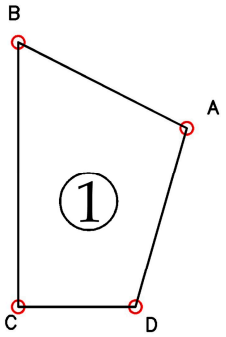
Acknowledgments: The authors would like to thank the Autonomous University of Querétaro, Faculty of Engineering, for the software resources used. Citlali Villalobos-García is grateful to the National Council for Humanities, Sciences, and Technologies (CECIHTI) for their scholarship grant, scholarship number 1,347,614.

Conflicts of Interest: The authors declare no conflicts of interest.

Appendix A

Appendix A.1

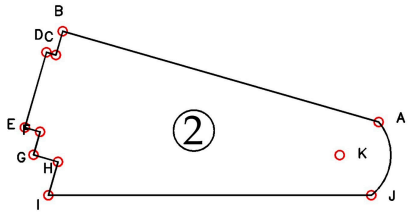
This appendix contains the cartesian coordinates for the representations of each of the surrounding buildings. The coordinates are described on a two-dimensional plane with x- and z-axes. Each box contains the dimensions of the sides for each building.



CONSTRUCTION DIAGRAM

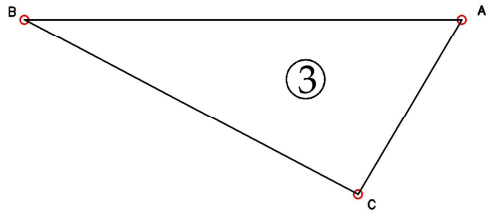
SIDE		COURSE	DISTANCE	V	COORDINATES	
EST	PV				Z	X
				A	7.7400	62.7900
A	B	N 63°00'00.98" W	37.138	B	24.6000	29.7000
B	C	S 00°00'00" E	52.000	C	−27.4000	29.7000
C	D	N 90°00'00" E	23.000	D	−27.4000	52.7000
D	A	N 16°01'14.66" E	36.560	A	7.7400	62.7900
AREA = 1,264.450 m2						

Figure A1. *Cont.*



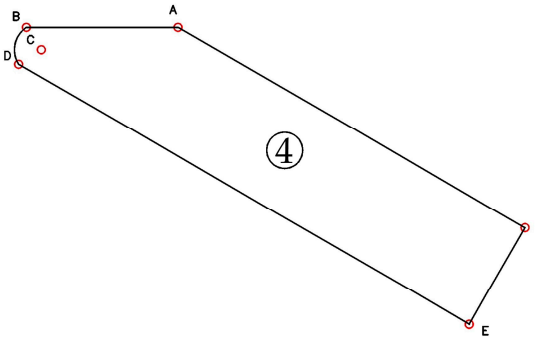
CONSTRUCTION DIAGRAM

SIDE EST	SIDE PV	COURSE	DISTANCE	V	COORDINATES Z	COORDINATES X
				A	−9.5736	154.7355
A	B	N 73°58'41.11" W	90.449	B	15.3908	67.7998
B	C	S 16°01'54.41" W	6.797	C	8.8586	65.9228
C	D	N 73°58'48.98" W	2.700	D	9.6037	63.3277
D	E	S 16°01'28.60" W	21.500	E	−11.0606	57.3927
E	F	S 73°58'11.16" E	4.360	F	−12.2646	61.5832
F	G	S 16°01'25.00" W	6.571	G	−18.5799	59.7695
G	H	S 73°56'36.74" E	7.001	H	−20.5163	66.4975
H	I	S 16°01'44.77" W	9.562	I	−29.7065	63.8572
I	J	N 89°59'44.91" E	88.852	J	−29.7000	152.7087
J	A	N 05°45'01.81" E CENTER OF CURVE DELTA = 92°7'51.64" RADIO = 14.045	20.228 CURVE LENGTH = 22.584 SUB.TAN.= 14.577	A K	−9.5736 −18.6604	154.7355 144.0264
AREA = 3,120.381 m2						



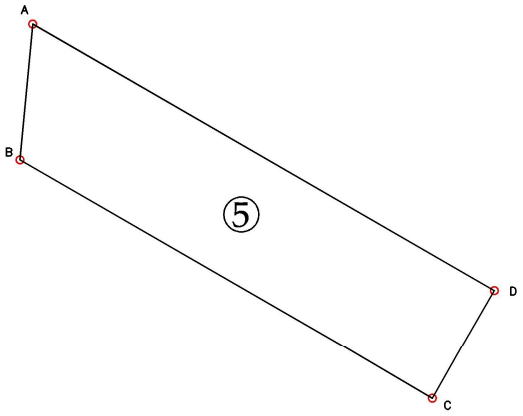
CONSTRUCTION DIAGRAM

SIDE EST	SIDE PV	COURSE	DISTANCE	V	COORDINATES Z	COORDINATES X
				A	−48.6400	180.5700
A	B	N 90°00'00" W	127.870	B	−48.6400	52.7000
B	C	S 62°24'40.70" E	110.052	C	−99.6076	150.2389
C	A	N 30°45'25.60" E	59.310	A	−48.6400	180.5700
AREA = 3,258.614 m2						



CONSTRUCTION DIAGRAM

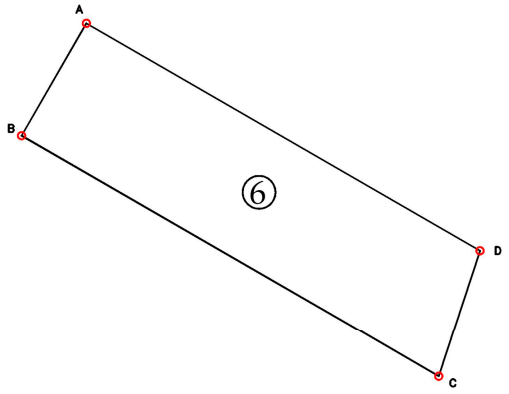
SIDE EST	SIDE PV	COURSE	DISTANCE	V	COORDINATES Z	COORDINATES X
				A	−48.6400	35.4000
A	B	N 90°00'00" W	47.300	B	−48.6400	−11.9000
B	D	S 11°49'43.10" W CENTER OF CURVE DELTA = 88°54'39.75" RADIO = 8.386	11.746 CURVE LENGTH = 13.013 SUB.TAN.= 8.228	D C	−60.1363 −55.6151	−14.3077 −7.2454
D	E	S 59°59'59.99" E	162.300	E	−141.2863	126.2482
E	F	N 30°00'00.13" E	34.810	F	−111.1400	143.6532
F	A	N 60°00'00.02" W	125.000	A	−48.6400	35.4000
AREA = 5,291.743 m2						



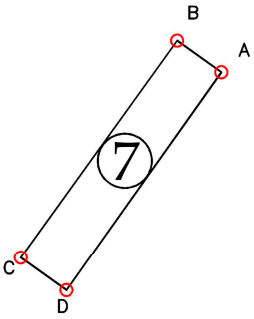
CONSTRUCTION DIAGRAM

SIDE EST	SIDE PV	COURSE	DISTANCE	V	COORDINATES Z	COORDINATES X
				A	−75.3587	−27.5419
A	B	S 05°20'00.37" W	43.873	B	−119.0421	−31.6200
B	C	S 59°59'59.98" E	153.190	C	−195.6371	101.0464
C	D	N 29°59'59.83" E	39.870	D	−161.1086	120.9814
D	A	N 60°00'00.07" W	171.500	A	−75.3587	−27.5419
AREA = 6,472.696 m2						

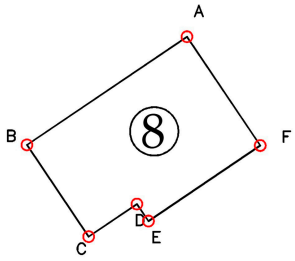
Figure A1. *Cont.*



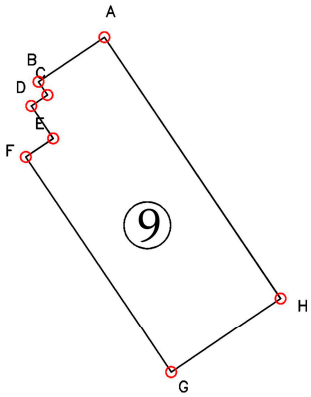
CONSTRUCTION DIAGRAM						
SIDE		COURSE	DISTANCE	V	COORDINATES	
EST	PV				Z	X
				A	−126.2301	−35.7700
A	B	S 30°00'00.01" W	44.280	B	−164.5777	−57.9100
B	C	S 60°00'00.01" E	164.900	C	−246.8777	84.5378
C	D	N 18°08'19.17" E	48.246	D	−203.8801	98.7237
D	A	N 59°59'59.97" W	188.300	A	−126.2301	−35.7700
AREA = 7,082.562 m2						



CONSTRUCTION DIAGRAM						
SIDE		COURSE	DISTANCE	V	COORDINATES	
EST	PV				Z	X
				A	−121.1355	−135.4568
A	B	N 54°31'51.59" W	11.260	B	−114.6018	−144.6272
B	C	S 35°51'05.52" W	55.401	C	−159.5066	−177.0750
C	D	S 54°31'52.18" E	11.630	D	−166.2550	−167.6032
D	A	N 35°28'07.77" E	55.400	A	−121.1355	−135.4568
AREA = 634.049 m2						

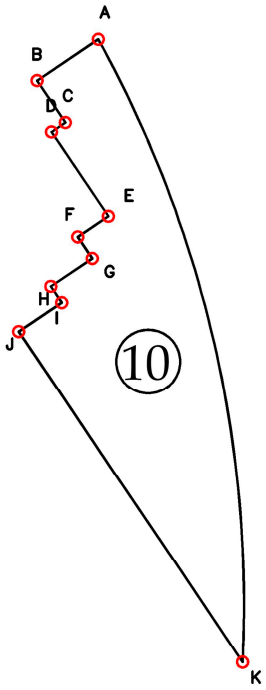


CONSTRUCTION DIAGRAM						
SIDE		COURSE	DISTANCE	V	COORDINATES	
EST	PV				Z	X
				A	−26.2600	−158.8000
A	B	S 55°59'51.43" W	44.776	B	−51.3000	−195.9200
B	C	S 33°59'37.94" E	25.630	C	−72.5500	−181.5900
C	D	N 55°59'31.50" E	13.499	D	−65.0000	−170.4000
D	E	S 34°01'27.64" E	4.754	E	−68.9400	−167.7400
E	F	N 56°00'00.03" E	31.277	F	−51.4500	−141.8100
F	A	N 33°59'55.11" W	30.384	A	−26.2600	−158.8000
AREA = 1,296.314 m2						



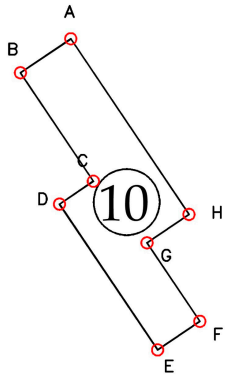
CONSTRUCTION DIAGRAM						
SIDE		COURSE	DISTANCE	V	COORDINATES	
EST	PV				Z	X
				A	40.8700	−204.0800
A	B	S 55°59'39.49" W	19.132	B	30.1700	−219.9400
B	C	S 33°58'45.22" E	3.847	C	26.9800	−217.7900
C	D	S 56°00'14.44" W	4.696	D	24.3544	−221.6832
D	E	S 34°00'42.09" E	9.427	E	16.5400	−216.4100
E	F	S 55°56'57.15" W	7.930	F	12.1000	−222.9800
F	G	S 34°00'10.16" E	62.496	G	−39.7100	−188.0300
G	H	N 55°59'58.97" E	31.760	H	−21.9500	−161.7000
H	A	N 34°00'16.64" W	75.779	A	40.8700	−204.0800
AREA = 2,283.252 m2						

Figure A1. *Cont.*



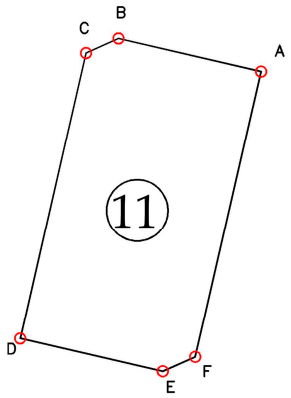
CONSTRUCTION DIAGRAM

SIDE EST	SIDE PV	COURSE	DISTANCE	V	COORDINATES Z	COORDINATES X
				A	123.7278	−162.1791
A	B	S 55°59'59.31" W	16.930	B	114.2606	−176.2147
B	C	S 33°59'59.80" E	11.600	C	104.6438	−169.7281
C	D	S 55°59'59.90" W	3.840	D	102.4965	−172.9116
D	E	S 34°00'00.65" E	23.300	E	83.1799	−159.8823
E	F	S 56°00'01.40" W	8.450	F	78.4547	−166.8878
F	G	S 34°00'01.49" E	5.950	G	73.5220	−163.5606
G	H	S 55°59'58.58" W	11.450	H	67.1192	−173.0530
H	I	S 34°00'06.65" E	4.470	I	63.4135	−170.5533
I	J	S 56°00'14.55" W	11.897	J	56.7617	−180.4165
J	K	S 33°59'51.01" E	91.682	K	−19.2480	−129.1522
K	A	N 13°00'25.19" W CENTER OF CURVE DELTA = 31°35'7.17" RADIO = 269.588	146.741 CURVE LENGTH= 148.615 SUB.TAN.= 76.249	A L	123.7278 −8.1460	−162.1791 −398.4220
AREA = 3,253.733 m2						



CONSTRUCTION DIAGRAM

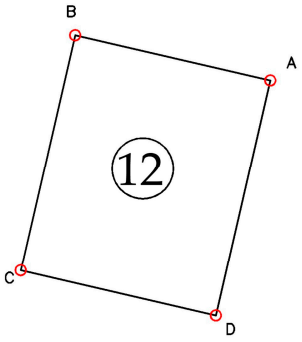
SIDE EST	SIDE PV	COURSE	DISTANCE	V	COORDINATES Z	COORDINATES X
				A	71.9000	−157.9600
A	B	S 56°03'03.59" W	13.502	B	64.3600	−169.1600
B	C	S 33°59'48.62" E	29.008	C	40.3100	−152.9400
C	D	S 55°59'42.10" W	9.083	D	35.2300	−160.4700
D	E	S 34°00'13.77" E	38.999	E	2.9000	−138.6600
E	F	N 56°00'54.89" E	11.324	F	9.2300	−129.2700
F	G	N 34°00'55.42" W	21.004	G	26.6400	−141.0200
G	H	N 55°59'58.63" E	11.266	H	32.9400	−131.6800
H	A	N 34°00'04.18" W	46.995	A	71.9000	−157.9600
AREA = 1,035.928 m2						



CONSTRUCTION DIAGRAM

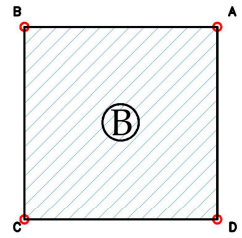
SIDE EST	SIDE PV	COURSE	DISTANCE	V	COORDINATES Z	COORDINATES X
				A	156.6382	143.3116
A	B	N 76°59'39.86" W	35.001	B	164.5150	109.2086
B	C	S 65°58'43.43" W	8.501	C	161.0543	101.4435
C	D	S 13°00'00.08" W	70.000	D	92.8484	85.6969
D	E	S 76°59'59.99" E	35.000	E	84.9751	119.7999
E	F	N 65°59'58.79" E	8.500	F	88.4324	127.5650
F	A	N 13°00'00.14" E	70.000	A	156.6382	143.3116
AREA = 3,104.300 m2						

Figure A1. *Cont.*



CONSTRUCTION DIAGRAM

SIDE EST	SIDE PV	COURSE	DISTANCE	V	COORDINATES Z	COORDINATES X
				A	104.5966	292.6437
A	B	N 77°00'00.15" W	48.000	B	115.3942	245.8740
B	C	S 13°00'00.19" W	58.000	C	58.8808	232.8268
C	D	S 76°59'59.83" E	48.000	D	48.0831	279.5966
D	A	N 12°59'59.76" E	58.000	A	104.5966	292.6437
AREA = 2,783.998 m2						



CONSTRUCTION DIAGRAM

SIDE EST	SIDE PV	COURSE	DISTANCE	V	COORDINATES Z	COORDINATES X
				A	29.7000	29.7000
A	B	N 90°00'00" W	59.400	B	29.7000	−29.7000
B	C	S 00°00'00" E	59.400	C	−29.7000	−29.7000
C	D	N 90°00'00" E	59.400	D	−29.7000	29.7000
D	A	N 00°00'00" E	59.400	A	29.7000	29.7000
AREA = 3,528.360 m2						

Figure A1. Cartesians coordinates for the surrounding buildings. Numbers indicate each building and letters their vertices coordinates.

Appendix A.2

In graphs (a) and (b), the simultaneity of the CFD simulations and results obtained through wind tunnel testing is evaluated using linear models, through a polyhedra mesh; in (c) and (d), the same parameters are evaluated through a polyhexacore mesh. The models and solution methods were evaluated, and the one giving results closest to those from the experimental studies was the k-ω-SST model with its simple solution method.

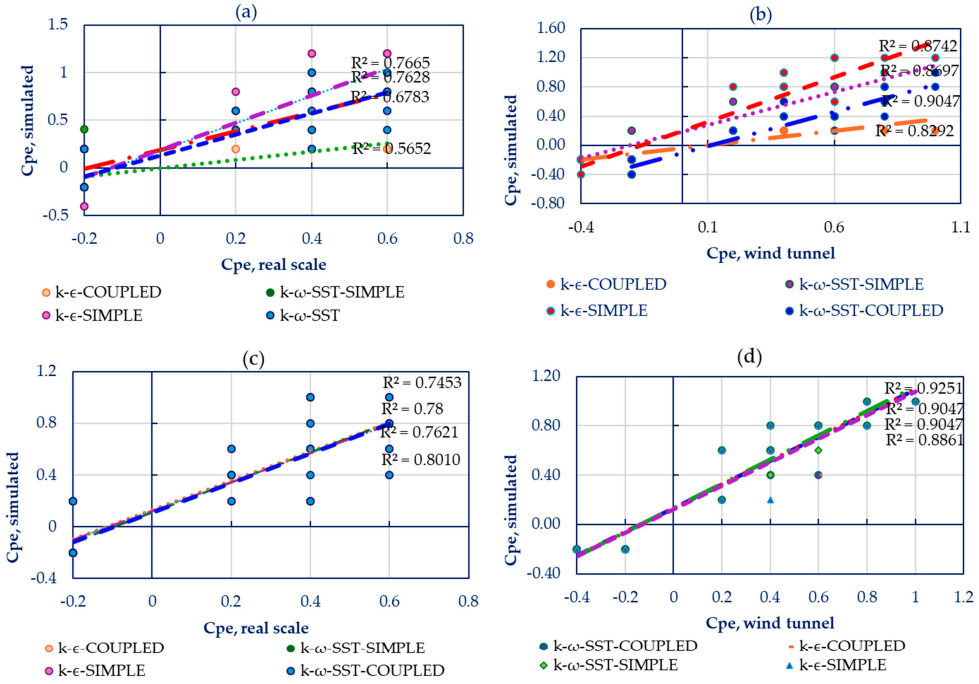


Figure A2. Comparison CFD vs. wind tunnel.

Appendix A.3

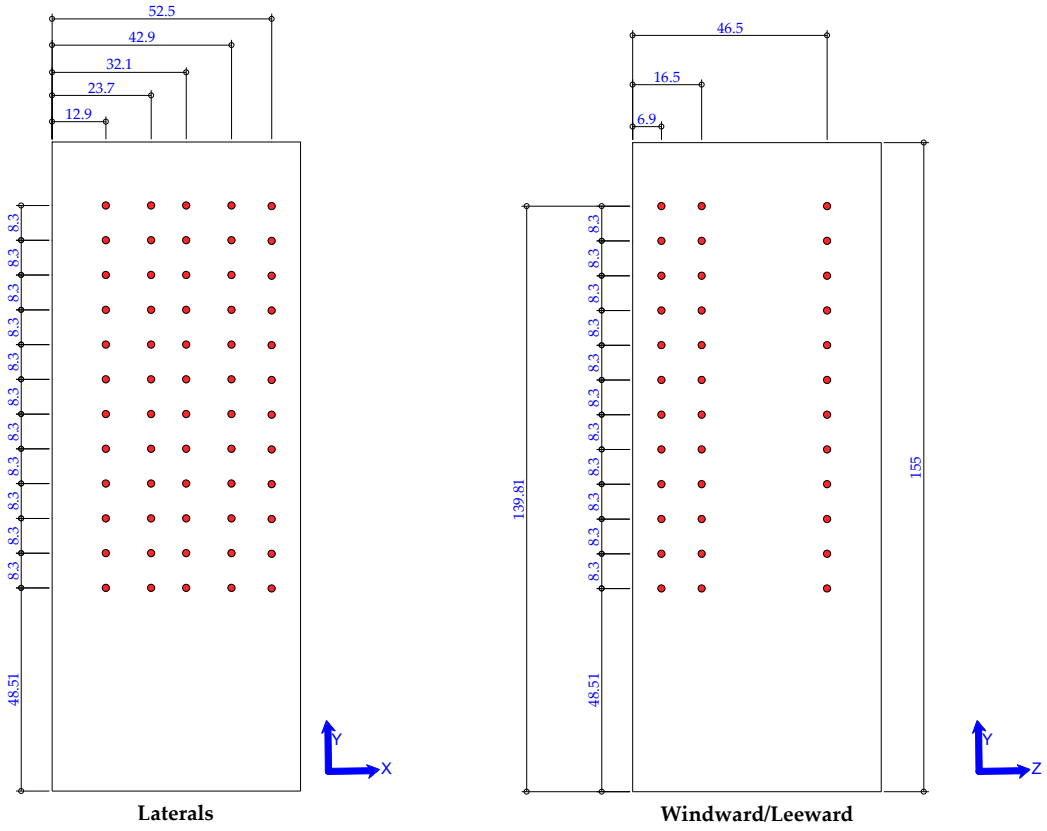


Figure A3. Locations of points on the surfaces of the building. Laterals: Surfaces that are oriented parallel to the direction of the fluid inlet.

References

1. Piralla, M. *Diseño Estructural [Structural Design]*, 2nd ed.; Limusa: Mexico City, Mexico, 2001.
2. Díaz, R.Y.B. *Mecánica de Estructuras [Structural Mechanics]*; CIMN: Barcelona, Spain, 2014.
3. Koks, E.E.; Haer, T. A high-resolution wind damage model for Europe. *Sci. Rep.* **2020**, *10*, 6866. [CrossRef]
4. Ouyang, Z.; Spence, S.M.J. Performance-based wind-induced structural and envelope damage assessment of engineered buildings through nonlinear dynamic analysis. *J. Wind Eng. Ind. Aerodyn.* **2021**, *208*, 104452. [CrossRef]
5. Tomás, A.; Morales, M. Revisión y estudio comparativo de la acción del viento sobre las estructuras empleando Eurocódigo y Código Técnico de la Edificación. *Inf. constr.* **2012**, *64*, 381–390. [CrossRef]
6. Zhao, Y.; Li, R.; Feng, L.; Wu, Y.; Gao, N. Boundary layer wind tunnel tests of outdoor airflow field around urban buildings: A review of methods and status. *Renew. Sustain. Energy Rev.* **2022**, *356*, 04031. [CrossRef]
7. *EN 1991-1-4*; Eurocode 1: Actions on Structures—Part 1–4: General Actions—Wind Actions. European Committee for Standardization: Brussels, Belgium, 2005.
8. *NTC (2023)*; Normas Técnicas Complementarias para Diseño por Viento. Secretarias de Obras y Servicios de la CDMX: Ciudad de México, México, 2023.
9. *ASCE 7*; Minimum design loads and associated criteria for buildings and other structures. American Society of Civil Engineers: Reston, VA, USA, 2023.
10. Iancovici, M.; Nica, G.B. Time-domain structural damage and loss estimates for wind loads: Road to resilience-targeted and smart buildings design. *Buildings* **2023**, *13*, 734. [CrossRef]
11. Coca-Obdulio. Daños del viento en zonas urbanas. *Arquit. Y Urban.* **2008**, *29*, 64–67.
12. Bustamante, C.; Jans, M.; Higueras, E. El comportamiento del viento en la morfología urbana y su incidencia en el uso estancial del espacio público, Punta Arenas, Chile. [Wind behavior in urban morphology and its impact on the leisure use of public space, Punta Arenas, Chile]. *AUS* **2017**, *6*, 28–33.
13. Lin, C.; Ooka, R.; Takakuwa, Y.; Kikumoto, H. Wind tunnel study of Parapet effects on rooftop wind environment with implications for safe urban-air-mobility operations. *Build. Environ.* **2025**, *284*, 113509. [CrossRef]
14. Taniike, Y. Interference mechanism for enhanced wind forces on neighboring tall buildings. *J. Wind Eng. Ind. Aerodyn.* **1992**, *42*, 1073–1083. [CrossRef]

15. Bailey, A.; Vincent, N.D.G. Wind-pressure on buildings including effects of adjacent buildings. *J. Inst. Civ. Eng.* **1943**, *20*, 243–275. [CrossRef]
16. Lam, K.M.; Leung, M.Y.H.; Zhao, J.G. Interference effects on wind loading of a row of closely spaced tall buildings. *J. Wind Eng. Ind. Aerodyn.* **2008**, *96*, 562–583. [CrossRef]
17. Ishida, Y.; Yoshida, A.; Yamane, Y.; Mochida, A. Impact of a single high-rise building on the wind pressure acting on the surrounding low-rise buildings. *J. Wind Eng. Ind. Aerodyn.* **2024**, *250*, 105742. [CrossRef]
18. Xamán, J. Dinámica De Fluidos Computacional Para Ingenieros. In *Computational Fluid Dynamics for Engineers*; Palibrio: Bloomington, IN, USA, 2016.
19. White, F.M. *Mecánica de Fluidos*; Mcgraw-Hill: Madrid, Spain, 2010.
20. Versteeg, H.K.; Malalasekera, W. *An Introduction to Computational Fluid Dynamics: The Finite Volume Method*, 2nd ed.; Pearson Education Limited: London, UK, 2007.
21. Baghaei Daemei, A.; Khotbehsara, E.M.; Nobarani, E.M.; Bahrami, P. Study on wind aerodynamic and flow characteristics of triangular-shaped tall buildings and CFD simulation in order to assess drag coefficient. *Ain Shams Eng. J.* **2019**, *10*, 541–548. [CrossRef]
22. Khalil, I.; Lakkis, I. *Computational Fluid Dynamics: An Introduction to Modeling and Applications*, 1st ed.; McGrawHill: New York, NY, USA, 2023; Available online: https://books.google.com.mx/books/about/Computational_Fluid_Dynamics_An_Introduc.html?id=eMCqEAAAQBAJ&redir_esc=y (accessed on 4 April 2024).
23. Liu, S.; Wuxuan, P.; Zhao, X.; Zhang, H.; Cheng, X.; Long, Z.; Chen, Q. Influence of surrounding buildings on wind flow around a building predicted by CFD simulations. *Build. Environ.* **2018**, *140*, 1–10. [CrossRef]
24. Kim, Y.C.; Yoshida, A.; Tamura, Y. Characteristics of surface wind pressures on low-rise building located among large group of surrounding buildings. *Eng. Struct.* **2012**, *35*, 18–28. [CrossRef]
25. Cheng, Z.; Wong, J.K.; Mercan, O. Evaluating the wind loads on high-rise buildings of various plan dimensions through numerical simulations. *Eng. Struct.* **2025**, *343*, 120981, 2025. [CrossRef]
26. Haan, F.L.; Wang, J.; Sterling, M.; Kopp, G.A. Experimentally estimating wind load coefficients for tornadoes–An alternative perspective. *J. Wind Eng. Ind. Aerodyn.* **2024**, *251*, 105811. [CrossRef]
27. Wijesooriya, K.; Mohotti, D.; Lee, C.-K.; Mendis, P. A technical review of computational fluid dynamics (CFD) applications on wind design of tall buildings and structures: Past, present and future. *J. Build. Eng.* **2023**, *74*, 106828. [CrossRef]
28. Idrissi, A.; El Mghari, H.; El Amraoui, R. CFD simulation advances in urban aerodynamics: Accuracy, validation, and high-rise building applications. *Results Eng.* **2025**, *26*, 105148. [CrossRef]
29. Liu, F.; Ren, Y.; Zhang, L.; Li, X. Impact of super high-rise buildings on wind comfort and safety of pedestrian wind environment: A case study in Shanghai, China. *Case Stud. Therm. Eng.* **2025**, *71*, 106197. [CrossRef]
30. Kikuchi, T.; Ohtake, K.; Takahashi, Y.; Watanabe, H.; Hidari, K.; Tanabe, S.; Nobe, T. Comparison of wind pressure coefficients between wind tunnel experiments and full-scale measurements using operational data from an urban high-rise building. *Build. Environ.* **2024**, *252*, 111244. [CrossRef]
31. ANSYS, Inc. Capítulo 4: Turbulencia» [Chapter 4: Turbulence], Ansys Fluent R2 2024. Accedido: 13 de enero de 2025. Available online: https://ansyshelp.ansys.com/public/account/secured?returnurl=/Views/Secured/corp/v242/en/flu_th/flu_th_sec_turb_kw_sst.html (accessed on 13 January 2025).
32. Fernández, M. *Técnicas Numéricas en Ingeniería de Fluidos: Introducción a la Dinámica de Fluidos Computacional (CFD) Por el Método de Volúmenes Finitos*; Reverté: Barcelona, Spain, 2012.
33. Fatchurrohman, N.; Chia, S.T. Performance of hybrid nano-micro reinforced mg metal matrix composites brake calliper: Simulation approach. *IOP Conf. Ser.: Mater. Sci. Eng.* **2017**, *257*, 012060. [CrossRef]
34. Huang, S.; Li, Q.S.; Xu, S. Numerical evaluation of wind effects on a tall steel building by CFD. *J. Constr. Steel Res.* **2007**, *63*, 612–627. [CrossRef]
35. Guevara Díaz, J.M. Cuantificación del perfil del viento hasta 100 m de altura desde la superficie y su incidencia en la climatología eólica. *Terra Nueva Etapa* **2013**, *29*, 81–101.
36. Kubilay, A.; Rubin, A.; Derome, D.; Carmeliet, J. Wind-comfort assessment in cities undergoing densification with high-rise buildings remediated by urban trees. *J. Wind Eng. Ind. Aerodyn.* **2024**, *249*, 105721. [CrossRef]
37. Montazeri, H.; Blocken, B. CFD simulation of wind-induced pressure coefficients on buildings with and without balconies: Validation and sensitivity analysis. *Build. Environ.* **2013**, *60*, 137–149. [CrossRef]

Disclaimer/Publisher's Note: The statements, opinions and data contained in all publications are solely those of the individual author(s) and contributor(s) and not of MDPI and/or the editor(s). MDPI and/or the editor(s) disclaim responsibility for any injury to people or property resulting from any ideas, methods, instructions or products referred to in the content.